Available online at www.sciencedirect.com
SCIENCE DIRECT®
Journal of Nuclear Materials 352 (2006) 202–208
journal of nuclear materials
www.elsevier.com/locate/jnucmat

Helium behaviour in waste conditioning matrices during thermal annealing

T.A.G. Wiss [a,*], J.-P. Hiernaut [a], P.M.G. Damen [a,1], S. Lutique [a,2], R. Fromknecht [b], W.J. Weber [c]

[a] European Commission, Joint Research Centre, Institute for Transuranium Elements, P.O. Box 2340, 76125 Karlsruhe, Germany
[b] Institut für Festkörperphysik, Forschungszentrum Karlsruhe, Postfach 3640, D-76021 Karlsruhe, Germany
[c] Pacific Northwest National Laboratory, P.O. Box 999, K8-93, Richland, WA 99352, USA

Abstract

Reprocessing of spent fuel produces high level waste including minor actinides and long living fission products that might be disposed in waste conditioning matrices. Several natural mineral phases were proven to be able to incorporate fission products or actinides in their crystalline structure for long periods of time. In this study, synthetic compounds of zirconolite ($CaZrTi_2O_7$) and pyrochlores ($Gd_2Ti_2O_7$ and $Nd_2Zr_2O_7$) were fabricated and doped with the short-lived alpha-emitter ^{244}Cm to increase the total amount of helium and damage generated in a laboratory time scale. Helium implantations were also used to simulate the damage caused by the alpha-decay and the build-up of helium in the matrix. The samples were annealed in a Knudsen cell, and the helium release profile interpreted in conjunction with radiation damage studies and previous analysis of annealing behaviour. Several processes like diffusion, trapping or phase changes could then be attributed to the helium behaviour depending on the material considered. Despite high damage and large amount of helium accumulated, the integrity of the studied materials was preserved during storage.

PACS: 51.20.+d; 61.72.Ww

1. Introduction

The nuclear industry generates from around 400 operating reactors a large stockpile of radioactive waste; mainly long lived Transuranium Elements (TRU-) such as Plutonium, Minor Actinides (Am, Np, Cm), and Long Lived Fission Products (LLFP) such as ^{129}I, ^{99}Tc, ^{135}Cs. It is estimated that around 300 000 tons of spent fuel has been produced in the past decade, with 1% of Pu (3000 tons), 0.1% MA, (300 tons), and 400 tons of LLFP. Recycling of ^{239}Pu in MOX fuel is a valuable solution. However, the Pu inventory is potentially too high and disposal of a part of this Pu is also considered. Several compounds have been taken into account to host the different radionuclides with the aim to immobilize them in geological repositories.

* Corresponding author. Tel.: +49 7247 951 447; fax: +49 7247 951 99447.
E-mail address: wiss@itu.fzk.de (T.A.G. Wiss).
[1] Current address: Nederlands Meetinstituut, Thijsseweg 11, 2629 JA Delft, The Netherlands.
[2] Current address: CEA, DEN/DEC/SPUA/LTEC, C.E.N Cadarache, Bât. 717, 13108 Saint Paul-lez-Durance, France.

0022-3115/$ - see front matter © 2006 Elsevier B.V. All rights reserved.
doi:10.1016/j.jnucmat.2006.02.055

Natural minerals were proven to be able to incorporate actinides in their crystalline structure for billion of years. It is the case for e.g., zirconolite ($CaZrTi_2O_7$) a uranium-bearing accessory mineral, found in a wide range of terrestrial and lunar rocks. It can accommodate high proportions of refractory elements, including U and Th, and it is the main host of the actinides and rare earth elements (REEs) in SYNROC, a synthetic rock proposed by the Australian Nuclear Science and Technology Organization (ANSTO) as a radioactive waste conditioning matrix [1]. SYNROC is composed of titanate minerals chosen for their geochemical stability and collective ability to immobilise the radioactive elements in nuclear waste. Indeed the titanate pyrochlore were also shown to be able to incorporate large amounts of actinides. There are extensive studies reporting on the behaviour of e.g., pyrochlores against build-up of radiation damage [2,3]. Natural analogues were the first investigated samples, and it is generally agreed that this structure appears to be able to confine the actinides over geological time scales. It was also shown that the zirconate were more radiation resistant than the titanate pyrochlore.

However, the long term behaviour of such containment matrices is strongly affected by radiogenic helium formation as well as by self-irradiation effects due to radioactive decay of the incorporated actinides. Ascertaining whether the helium generated in these materials can be accommodated in the lattice or at trapping sites without adversely affecting the material integrity or whether helium will migrate, possibly increasing the pressure on the next confinement barrier is of major importance to overall waste package behaviour.

The following compounds have therefore been considered in this study: zirconolite ($CaZrTi_2O_7$) that can accommodate the Ln and tri- and tetravalent An in the Ca and Zr sites of the monoclinic structure and pyrochlores ($Gd_2Ti_2O_7$, $Gd_2Zr_2O_7$ and $Nd_2Zr_2O_7$).

2. Experimental procedure

$Nd_2Zr_2O_7$ samples were prepared at ITU by precipitation from a solution of zirconium oxi-chloride $ZrOCl_2 \cdot 8H_2O$ and neodymium nitrate $Nd(NO_3)_3 \cdot 6H_2O$ with the right concentration using a sol–gel method. Pellets were obtained by pressing resulting beads after calcination for 1 h at 1073 K and a compaction/milling step. They were sintered in air for 8 h at $T = 1923$ K. X-ray diffraction revealed only a pyrochlore phase with a lattice parameter of 1.070 nm. Pellet densities were measured by a geometrical method and showed 97% of the theoretical density. The theoretical density (TD = 6325 kg m^{-3}) was calculated from the lattice parameter value measured. $Nd_2Zr_2O_7$ pellets were used to prepared bulk slices which preparation is described in Ref. [4]. The extracted slices were annealed for 2 h at 1473 K in air.

$Gd_2Ti_2O_7$ and $Gd_2Zr_2O_7$ samples were prepared at ANSTO by pressing powder obtained by a sol–gel method [5]. The pellets were sintered at 1873 K for 2 h under reducing atmosphere and bulk slices were subsequently polished and annealed at 1623 K for 48 h under an oxidising atmosphere. The pellets have a density of 97% and 82% of the theoretical densities, and a lattice parameter of 1.0185 and 1.053 nm, for $Gd_2Ti_2O_7$ and $Gd_2Zr_2O_7$, respectively.

The materials used in the present study were treated according to two procedures: Helium implantation (titanates and zirconates pyrochlores) and doping with ^{244}Cm.

2.1. Helium implantation

$Nd_2Zr_2O_7$, $Gd_2Ti_2O_7$ and $Gd_2Zr_2O_7$ disks have been implanted at the Van de Graaf accelerator of the Institut für Festkörper Physik (Forschungszentrum Karlsruhe). The irradiation was performed at room temperature with 1 MeV helium ions. The He-beam diameter was around 1 mm and the fluence was determined from charge integration measurements. The implantation depth and distribution was calculated using the SRIM2000 code [6] as well as the total number of displacements (dpa) at the damage peak. A threshold displacement energy of 50 eV for titanates and zirconates was chosen [7]. Fig. 1 shows the Gaussian distribution of the helium centered at a depth of 2.5 ± 0.2 μm. The damage profile for the ion implantation fluence of 10^{15} cm^{-2} has a peak value of 0.03 displacements per atoms (dpa) and is slightly shifted to the surface relative to the implanted helium profile.

2.2. Doping with ^{244}Cm

The preparation of pyrochlore ($Gd_2Ti_2O_7$) and zirconolite ($CaZrTiO_2$) doped with ^{244}Cm is described in reference [8]. The total quantity of helium generated in the samples between the end

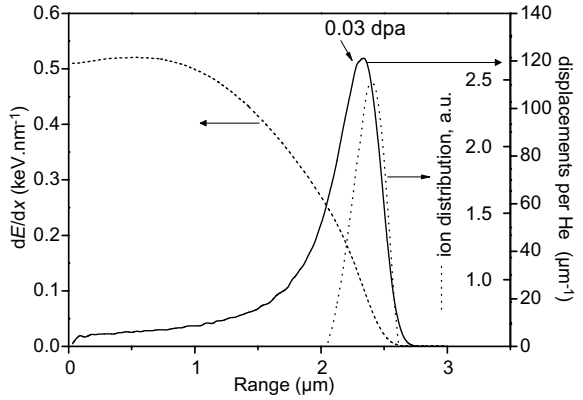

Fig. 1. SRIM2000 calculation of the range and distribution (dotted line) of 1 MeV He-ions in $Nd_2Zr_2O_7$ samples. The displacements distribution (full line) is shown on the same graph indicating a maximum of 0.03 dpa in the damage peak centred at a depth of 2.3 μm. The electronic energy loss is indicated on the left axis.

of preparation and the annealing experiments in the Knudsen cell (~20 years) was calculated with the Nuclides.net code [9]. Table 1 summarizes the helium content in the different studied materials at the time the experiments were carried out. The total quantity of helium generated during this time interval is slightly higher than that produced in a standard MOX fuel after 1000 years disposal, i.e., ~1 $cm^3\ g^{-1}$ [10].

2.3. Knudsen cell measurements

Fragments of some milligrams of the Cm-doped material or thin implanted disks have been annealed in an Al_2O_3 Knudsen cell (KC) up to 2000 K with a heating rate of 30 K min^{-1}. The species (mainly He) escaping from the sample were analysed on line by mass-spectrometry (a description of the apparatus can be found in Ref. [11]).

The release profiles were evaluated as functions of time/temperature, and some of the samples observed by scanning electron microscopy (SEM) before and after annealing. The SEM used in this study is a Philips XL40 mounted inside a glove-box for the handling of radioactive materials.

3. Discussion

3.1. Implanted specimens

Fig. 2 shows the release curves for the three helium implanted specimens. In the case of $Nd_2Zr_2O_7$ a symmetric release peak attributable to a diffusion process is observed starting at about 600 K. Its shape is, however, not typical and should rather present a sharp increase followed by a tail. This difference has been explained by Damen [12] as being a consequence of small grain size. Indeed, the range of the implanted helium atoms exceeds many time the

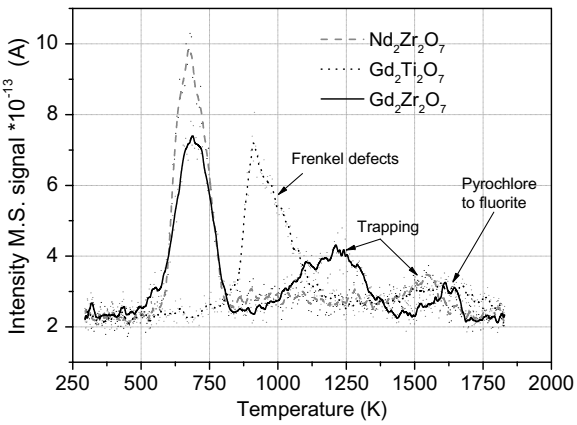

Fig. 2. Intensity of the helium mass-spectrometer (MS) signal and fractional release from $Nd_2Zr_2O_7$, $Gd_2Zr_2O_7$ and $Gd_2Ti_2O_7$ samples implanted with a He-ion fluence of 10^{15} cm^{-2}.

Table 1
Main characteristics of the samples used in the helium release study and values of pre-exponential factor and activation enthalpies of diffusion

	$(CaZrCm)Ti_2O_7$	$(Gd, Cm)_2Ti_2O_7$	$Nd_2Zr_2O_7$	$Gd_2Zr_2O_7$	$Gd_2Ti_2O_7$
Density (g cm^{-3})			6.135	5.7	6.37
T_{meling} (K)	–	–	2573	1823[a]	–
$T_{recrystallization}$ (K)	~870	~1020	~1040[b]	~950[b]	–
He in sample (mol)	4.62×10^{-7}	3.95×10^{-7}	1.7×10^{-10}	1.7×10^{-10}	1.7×10^{-10}
D_0 ($cm^2\ s^{-1}$)	–	–	0.586	0.156, 1.54	0.0589
[c]ΔH_a (eV)	2.61, ~0.1	3.17, ~0.1	1.17, 2.32	1.10, 2.33	2.10

[a] Phase transition pyrochlore–fluorite.
[b] Results obtained by Differential Thermal Analysis [4].
[c] Energy obtained after fitting with the program EFFUS [10].

grain size and as a consequence diffusion along the grain boundaries is enhanced toward the surface.

A second peak appears at around 1400 K attributed to release of helium trapped in extended defects or bubbles.

In the case of $Gd_2Zr_2O_7$, the release profile presents two release peaks at about the same temperatures as the previous specimens, but in this case a third peak appears at 1000 K. This compound is peculiar in the series of lanthanide zirconates since it undergoes a phase transition from pyrochlore to fluorite at a temperature of 1823 K. This compound was sintered for 2 h at 1873 K during its synthesis, which is a temperature slightly higher than the temperature for the transition from pyrochlore to fluorite. The resulting material had fluorite-type structure, but subsequent annealing at 1623 K for 48 h resulted in a transformation back to the pyrochlore structure with a lattice parameter measured of 1.0533 nm. However, it could not be excluded that a partial fluorite structure has remained in this material. Thus, the additional release peak at ~1000 K could be explained by the presence of this supplementary phase. Indeed, the first release peak starting at around 600 K would correspond to the release from the pyrochlore phase also influenced by the grain size, as for the $Nd_2Zr_2O_7$. The last peak at ~1500 K would then correspond to the release from trapping sites.

The release profile from implanted $Gd_2Ti_2O_7$ is quite different. The first peak occurring at 900 K is asymmetric with a sharp increase followed by a moderate tail. This shape is typically associated to a diffusion process with, however, a too sharp increase. This type of release has been shown for Xe in an amorphized $MgAl_2O_4$ sample [13]. Implantation of $Lu_2Ti_2O_7$ with 50 keV He-ions at a fluence of 4.6×10^{14} cm^{-2} does not result in amorphization. This is expected since this composition exhibits a strong dependence of the critical amorphization temperature on the incident ion mass [14]. Consequently this material does not amorphize above 300 K when irradiated with He. On-the-other-hand, $Gd_2Ti_2O_7$, under ion irradiation exhibits a critical temperature of ~1000 K and critical dose of 0.15 dpa at 300 K which does not depend on the ion mass [14]. This suggests that the He implantation in the present study probably resulted in some amorphization at the damage peak. Thus, the type of release observed at 900 K may be associated with some recrystallization of this buried amorphous material. At the lower irradiation doses between the damage peak and the surface, anionic disordering and a redistribution of oxygen vacancies are expected [2,14]. These vacancies could trap the helium atoms which could be released by defect healing (850 K). The second peak at about 1500 K likely corresponds to the behaviour observed for $Nd_2Zr_2O_7$ and $Gd_2Zr_2O_7$, which is helium release from structural defects or bubbles.

The release profiles observed for the zirconates of the pyrochlore type are similar to those for yttria-stabilized zirconia (YSZ) and are starting at more or less the same temperature, depending on the implanted dose. The activation energy for the diffusion could be calculated from the release profiles.

The total quantity of helium released from the sample is modeled with the assumption that the initial profile is a Gaussian (evidenced by Neutron Depth Profiling for the case of helium implanted in YSZ [12,15,16]. The model is based on Eq. (1) where D is the diffusion coefficient, D_0 the pre-exponential factor, k Boltzmann constant and ΔH_a the activation enthalpy [17]. This model does not account for radiation damage and supposes that diffusion occurs isotropically, although there is a preferential diffusion towards the surface. The fractional release curves can be fitted and the value for D_0 and ΔH_a deduced. Table 1 summarizes the value for D_0 and ΔH_a for the three implanted materials studied. In the case of gadolinium zirconate a theoretical equation for a diffusion in two steps (different D) has been used.

$$D = D_0 \cdot e^{-\left(\frac{\Delta H_a}{kT}\right)} \quad (1)$$

Table 1 lists the different values of D_0 and ΔH_a calculated. The activation enthalpy for the diffusion of He in $Nd_2Zr_2O_7$ and the first value for $Gd_2Zr_2O_7$ are similar (~1.13 ± 0.04 eV). Helium diffusion in zirconates appears to be more efficient than in titanates. The second value of the diffusion enthalpy for $Gd_2Zr_2O_7$ (release from the fluorite phase) is much higher highlighting the better retention capacity of this structure.

3.2. Cm-doped samples

The release curve of the $Gd_2Ti_2O_7$ pyrochlores doped with ^{244}Cm is shown in Fig. 3 together with the corresponding fractional release. The release curve of the He-implanted specimen has been plotted in the same graph for comparison. It is clear that the two stages of release are common to the two types of specimens i.e., a first one occurring between

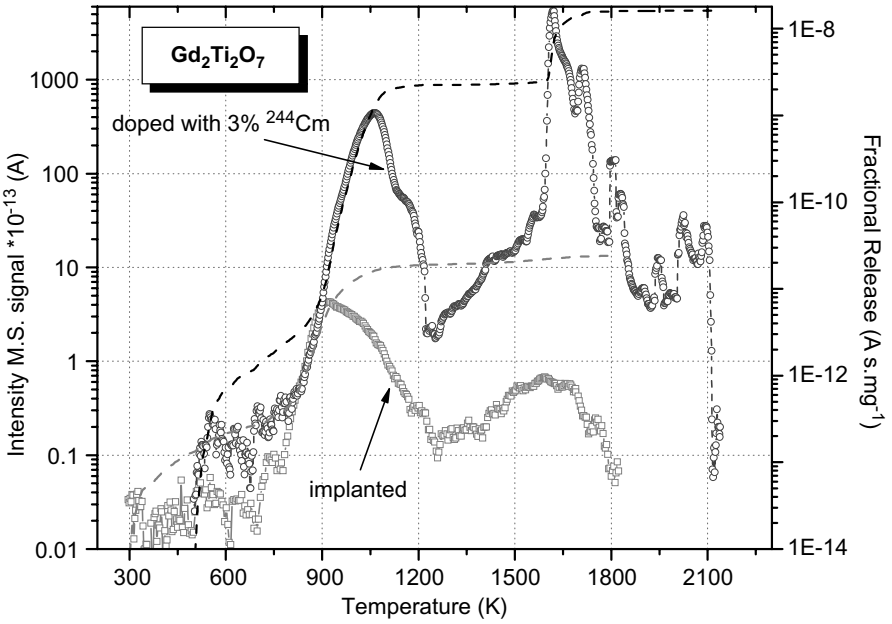

Fig. 3. Intensity of the helium mass-spectrometer (MS) signal and fractional release (dashed curves) from $Gd_2Ti_2O_7$ samples implanted at a He-ion fluence of 10^{15} cm^{-2} and doped with 3 wt% ^{244}Cm.

~900 and 1200 K and a second one between 1400 and 1800 K. However, the total quantity of helium and the overall damage are of completely different kind and amplitude. It should be noted that the ratio of the He (and fractional release) measured on both samples is compatible with the He quantities present in these samples (about 3 orders of magnitude). It further shows the good He retention capacity of these samples. The long plateau in the $(Gd,Cm)_2Ti_2O_7$ until the second stage of release is probably due to the fact that $Gd_2Ti_2O_7$ recrystallizes into the pyroclore structure, which has struc-

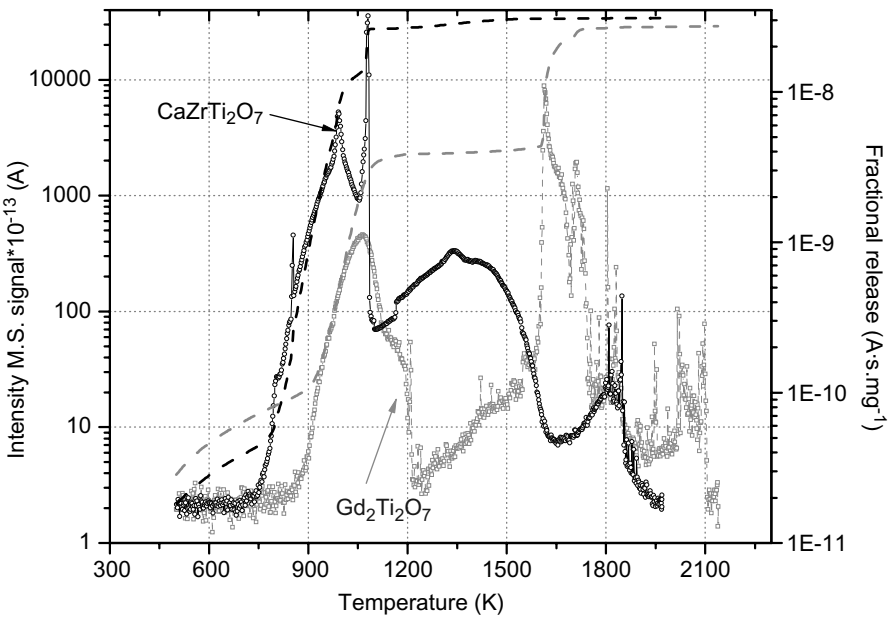

Fig. 4. Intensity of the helium mass-spectrometer (MS) signal (full lines) and fractional release (dashed curves) from $Gd_2Ti_2O_7$ and $CaZrTi_2O_7$ samples doped with 3 wt% ^{244}Cm.

tural oxygen vacancies that can trap the He. Over this temperature range the $(Gd, Cm)_2Ti_2O_7$ unit cell decreases due to ordering and defect recovery, but maintains a high concentration of structural O vacancies. In this material, the second stage of He release is probably due to the detrapping of He from the structural O vacancies.

In Fig. 4 the Mass-Spectrometer (MS) signal and fractional release of helium from $Gd_2Ti_2O_7$ (pyrochlore) and $CaZrTi_2O_7$ (zirconolite) samples doped with 3 wt% ^{244}Cm are presented. From the Normalized Fractional Release (NFR) data it is clear that the onset of significant He release is closely associated with the onset of recrystallization and densification measured previously [8]. In the case of zirconolite, earlier recovery studies showed that zirconolite initially recrystallized to a pseudo cubic structure, which may have some structural vacancies, and did not recrystallize into the stable monoclinic structure up to about 1450 K. Thus, the He release between 1100 and 1500 K in zirconolite may be associated with the transformation to the stable monoclinic structure, which has no structural vacancies. At about 1750 K detrapping occurs and the release is complete. Fig. 5 shows two SEM micrographs of the material before and after annealing, showing the recrystallization process occuring at about 870 K. On the first micrograph of the as stored material it can be noticed that the initial grains are still well shaped, although they appear to be fully restructured when looking at higher magnification.

As previously mentioned, while comparing the implanted and Cm-doped pyrochlores one can see in Fig. 4 that the end release of the two types of

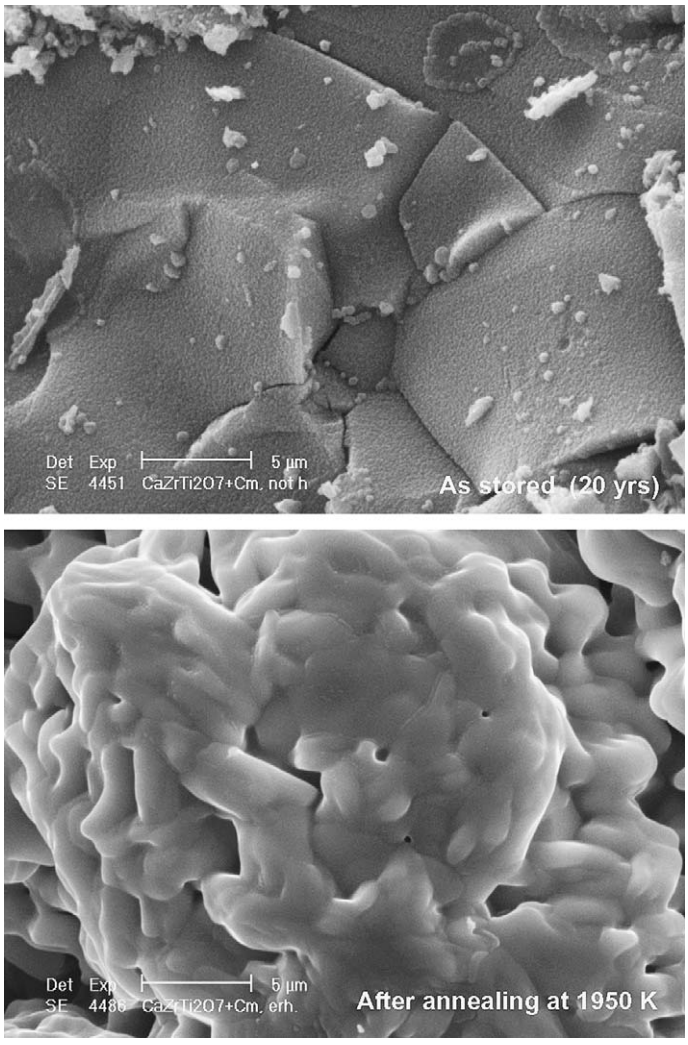

Fig. 5. SEM micrograph of a $CaZrTi_2O_7$ sample as stored for ~20 years and after annealing at 1950 K.

coumpounds are in good agreement with the quantities of He, given in Table 1, proving their good He retaining capacity.

The activation enthalpies of diffusion deduced from the fitting of the release curves (first peak on the release curves) for both Cm-doped specimens are high compared to those of the implanted specimens. It might be attributed to the recrystallization process occurring at the concerned temperature. While the implanted specimens are only locally disturbed by helium (damage peak, precipitated helium), the doped specimens are fully amorphized. The helium release is then directly linked to the recrystallization of the matrix. It should be noted that this diffusion process addresses only ~20% of the helium since the rest of the gas precipitates or remains trapped in the 'recrystallized' matrix until its final release starting above 1200 K. It is not proven that the retained gas is trapped in bubbles or in defects of the recrystallized matrix. However, the last stages seems to indicate that the release occurs by burst possibly attributable to the opening of channels in the structure.

4. Conclusion

In this study, synthetic compounds of zirconolite and pyrochlores were fabricated and doped with the short lived alpha-emitter ^{244}Cm ($T_{1/2} = 18.11$ years) to increase the total amount of helium and damage generated in a laboratory time scale. Helium implantations were also used to simulate the damage caused by the alpha-decay and the build-up of helium in the matrix. The samples were annealed in a Knudsen cell and the helium release profile qualitatively interpreted. Radiation damage studies were performed showing amorphization for all the materials doped with Cm. The Normalized Fractional Release data show that the onset of significant He-release is closely associated with the onset of recrystallization and densification. Several processes like diffusion, trapping or phase changes could then be attributed to the helium behaviour depending on the material considered. It is worth noting that the integrity of the studied materials was preserved during storage. The pyrochlore structure had been extensively studied to determine its resistance to alpha-damage build-up and this complementary study on helium behaviour shows the ability for this type of compound to accommodate large quantities of helium. However, the present investigation was performed on samples stored at room temperature. One would have to account for repository storage conditions (a temperature of 500 K could be easily reached) to assess more accurately the behaviour of such matrices since the helium release e.g., starts at rather low temperatures.

Acknowledgements

The authors are thankful to F. Capone and J.Y. Colle for the Knudsen cell measurement and to H. Thiele for the SEM analysis. The help for specimen implantation by the team at the Van de Graaf of IFP is also associated to these acknowledgements. B. Begg at ANSTO is kindly acknowledged for providing some of the pyrochlore samples.

References

[1] A.E. Ringwood, Fortschr. Mineral. 58 (1980) 149.
[2] R.C. Ewing, W.J. Weber, J. Lian, J. Appl. Phys. 95 (2004) 5949.
[3] W.J. Weber, R.C. Ewing, C.R.A. Catlow, T. Diaz de la Rubia, L.W. Hobbs, C. Kinoshita, Hj. Matzke, A.T. Motta, M. Nastasi, E.K.H. Salje, E.R. Vance, R.J. Zinkle, J. Mater. Res. 13 (1998) 1434.
[4] S. Lutique, PhD thesis, University Paris XI, Orsay, 2003.
[5] S.X. Wang, B.D. Begg, L.M. Wang, R.C. Ewing, W.J. Weber, K.V. Godivan Kutty, J. Mater. Res. 14 (1999) 4470.
[6] J.F. Ziegler, J.P. Biersack, U.L. Littmark, The Stopping Power and Range of Ions in Solids, Pergamon, New York, 1985.
[7] K.L. Smith, M. Collela, R. Cooper, E.R. Vance, J. Nucl. Mater. 321 (2003) 19.
[8] W.J. Weber, J.W. Wald, Hj. Matzke, Mater. Lett. 3 (1985) 173.
[9] J. Magill, Nuclides.net, An Interactive Environment for Computations on Radionuclides and Their Radiation, Springer Verlag, 2002.
[10] C. Ronchi, J.-P. Hiernaut, J. Nucl. Mater. 325 (2003) 1.
[11] F. Capone, J.-P. Hiernaut, M. Martellenghi, C. Ronchi, Nucl. Sci. Eng. 124 (1996) 436.
[12] P.M.G. Damen, Helium and fission gas behaviour in magnesium aluminate spinel and zirconia for actinide transmutation, ISBN 90-407-2446-6, DUP Science, Delft, The Netherlands.
[13] P.M.G. Damen, A. van Veen, Hj. Matzke, H. Schut, J.A. Valdez, C.J. Wetteland, K.E. Sickafus, J. Nucl. Mater. 306 (2002) 180.
[14] J. Lian, L. Wang, J. Chen, K. Sun, R.C. Ewing, J. Matt Farmer, L.A. Boatner, Acta Materialia 51 (2003) 1493.
[15] P.M.G. Damen, Hj. Matzke, C. Ronchi, J.P. Hiernaut, T. Wiss, R. Fromknecht, A. van Veen, F. Labohm, Nucl. Instrum. Meth. B 191 (2002) 571.
[16] P.M.G. Damen, A. van Veen, F. Labohm, H. Schut, M.A. van Huis, J. Nucl. Mater. 319 (2003) 65.
[17] J. Crank, The Mathematics of Diffusion, Oxford University, 1956;
H.S. Carslaw, J.C. Jaeger, Conduction of Heat in Solids, Oxford University, 1971.